ACS APPLIED MATERIALS & INTERFACES

Research Article

www.acsami.org

# High Efficiency of Poly(3-hexylthiophene)/[6,6]-phenyl $C_{61}$ Butyric Acid Methyl Ester Bulk Heterojunction Solar Cells through Precrystallining of Poly(3-hexylthiophene) Based Layer

Lie Chen,[†,‡] Peishan Wang,[†] and Yiwang Chen*[,†,‡]

[†]Institute of Polymers/Department of Chemistry and [‡]Jiangxi Provincial Key Laboratory of New Energy Chemistry, Nanchang University, 999 Xuefu Avenue, Nanchang 330031, China

**ABSTRACT:** An facile approach for improving device efficiency of poly(3-hexylthiophene) (P3HT)/[6,6]-phenyl $C_{61}$ butyric acid methyl ester ($PC_{61}BM$) bulk heterojunction solar cells is presented. This method is used by simply precasting a tiny thin P3HT layer with high crystallinity between PEDOT:PSS and photoactive P3HT:$PC_{61}BM$ layers. The high crystalline thin P3HT layers are casted from three different solvents such as dichloromethane (DCM), dichlorobenzene (*o*-DCB), and tetrahydrofuran (THF). It is demonstrated that THF used for thin P3HT layer preparation is a suitable solvent for yielding a high crystalline film, which is unreadily washed away during the solution processing of the active layer. The results indicate that the morphology of P3HT:$PC_{61}BM$ active layers strongly depend on the formation of P3HT buffer layer. A great morphology difference of P3HT:$PC_{61}BM$ is caused from crystallinity of P3HT buffer layers prepared by different solvents. The thin P3HT layer with high crystallinity can improve the crystalline degree of P3HT in the active layer, subsequently inducing the whole active layer to form a well self-assembled pathway for efficient charge transfer and transportation to their respective electrodes. Therefore, a dramatically enhanced short-circuit current density of the device is resulted. After optimization of thickness of the P3HT buffer layer, an improvement of the power conversion efficiency is obtained from 2.98% to 5.14%.

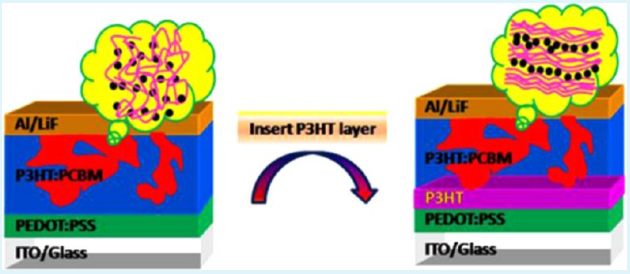


**KEYWORDS:** *crystallinity, morphology, conjugated polymers, solar cells*

## 1. INTRODUCTION

Polymer solar cells have been of great interest attribute to the property of low-cost, solution-based processing, and fabrication on the flexible substrates, which offer a crucial advantage over silicon solar cell.[1] During photoactive donor/acceptor composites, the blend of poly(3-hexylthiophene) (P3HT) with [6,6]-phenyl-$C_{61}$-butyric acid methyl ester ($PC_{61}BM$) has been intensively studied in recent years for polymer solar cells and has a power-conversion efficiency (PCE) of about 5%.[2] However, the efficiency is insufficient to meet the requirement of practice application. Great effort has been made toward improving the PCE of P3HT:$PC_{61}BM$ -based device.

The investigation of the morphology of the photoactive layer has been found to be a significant factor to obtain high PCE devices.[3−6] An optimum blend morphology should consist of a bicontinuous interpenetrating nanoscale network of both donor and acceptor materials produce a large amount of donor/acceptor interfaces. With such network, phase separated domains in the active layer offer not only interfaces for charge separation of photogenerated excitons but also percolation pathways for charge carrier transport to the respective electrodes, critically impact the device's PCE. Thermal-annealing is regarded as the optimum method to improve the efficiency of P3HT:$PC_{61}BM$-based solar cells, because it can improve the crystalline degree of the polymer to obtain higher mobility for holes,[7,8] and optimize formation of $PC_{61}BM$ aggregates at the same time.[9,10] Other methods have also been proposed to control the morphology of P3HT:PCBM blends, for instance, slow drying,[11] vapor annealing,[12] and additives.[13,14] However, recent works have shown that these procedures frequently led to in a vertical composition gradient of PCBM and P3HT with a profile of $PC_{61}BM$-rich blend near the poly(3,4-ethylenedioxythiophene):poly(styrene-sulfonate) (PEDOT:PSS) layer and P3HT-rich blend adjacent to the top surface of the composite film.[9] This structure is the opposite to that of the ideal donor-rich near the anode and acceptor-rich near the cathode. It is attributed that the acceptor contacts the anode or the donor contacts the cathode, charge recombination would be happened at the junction interface. This question has resulted in the application of a series processing techniques, for example, the use of an inverted cell structure,[15,16] the interface modification of the bottom layer with self-assembled layers,[9] and the insertion of a $C_{60}$ derivative layer between the active layer and the cathode.[17,18]

In addition, a P3HT buffer layer prepared by chlorobenzene between the poly(3,4-ethylenedioxythiophene)/poly-(styrenesulfonate) (PEDOT:PSS) layer and the active layer

Received: January 28, 2013
Accepted: June 13, 2013
Published: June 13, 2013

  

has been reported to improve the PCE.[19] It demonstrated that the thin P3HT layer created new contacts with those $PC_{61}BM$ molecules that are distributed near the bottom of the P3HT:$PC_{61}BM$ film, which increased the rate of generation of free carriers and the photocurrent density. Moreover, this layer increased the electron blocking capability of PEDOT:PSS, leading to a large increment of the rectification ratio of the cell. The performance was substantially improved to 5.05%. Unfortunately, the P3HT buffer layer was readily washed away with the solution processing of the active layer. To overcome this problem, Wei et al.[20] prepared a thin layer of P3HT using the electrochemical deposition method. They pointed out that this P3HT buffer layer was insoluble in all solvents; furthermore, it prevented the contact between the electron acceptor and the hole-collecting electrode, thereby eliminating carrier recombination at the active layer/anode interface. However, with respect to the solution processing, inconvenient electrochemical deposition only gave a PCE of 4.18%.

Since the morphology of the active layer is crucial for achieving high PCE device, if a high crystalline P3HT thin film is performed under the P3HT:$PC_{61}BM$ active layer, it not just only would possess the function of electron blocking layer and enlarge the heterojunction interface areas mentioned above, the high crystallinity of the P3HT should promote the strong aggregation and intermolecular $\pi$-packing of P3HT in the P3HT:$PC_{61}BM$ uplayer. Inspired by this, we demonstrate an useful and convenient method for controlling the morphology and crystallinity of P3HT:$PC_{61}BM$ blend films by simply precasting a tiny thin P3HT layer with high crystalline between PEDOT:PSS and photoactive layers and explore the impacts of P3HT layer on the morphology of photoactive layer and device performance. To carry out our studies, the tiny thin P3HT layer were very carefully prepared from three different solvents, such as dichloromethane (DCM), dichlorobenzene (*o*-DCB), and tetrahydrofuran (THF), to obtain high degree crystallinity, and to ensure the formation of the P3HT layer unreadily washed away during the solution processing of the active layer at the same time. We found that the morphology of P3HT:$PC_{61}BM$ active layers greatly depended on the formation of P3HT buffer layer. The thin P3HT layer with high crystallinity can improve the crystalline degree of P3HT in the active layer, consequently inducing the whole active layer to form a well self-assembled pathway for efficient charge transfer and transportation to their respective electrodes. After optimization of thickness of P3HT buffer layer prepared from THF, an improvement of the power conversion efficiency was obtained from 2.98% to 5.14%.

## 2. EXPERIMENTAL SECTION

**Materials.** Regioregular P3HT ($M_w$ = 48 300 g $mol^{-1}$, head-to-tail regioregularity > 90%) and $PC_{61}BM$ (99.5% purity) were obtained from Rieke Metals, Inc. and Nano-C, respectively. The solvents, 1,2-dichlorobenzene (*o*-DCB), tetrahydrofuran (THF), and dichloromethane (DCM) were all purchased from Sigma-Aldrich. Poly(3,4-ethylenedioxythiophene)/poly(styrenesulfonate) (PEDOT:PSS; Clevios, Heraeus PVP Al 4083) was used as hole transport layer. All chemicals were used as received without any further purification.

**Polymer Solar Cell Fabrication and Testing.** The polymer solar cells were fabricated on indium–tin oxide (ITO) coated glass substrates. The ITO glass was cleaned through sequential ultrasonic treatment in acetone, detergent, deionized water, and isopropanol, and then treated in an ultraviolet-ozone chamber for 10 min. Then a thin layer of PEDOT:PSS was spin-coated onto the ITO electrode at 4000 rpm (rpm: revolutions per minute) for 60 s to give a film thickness of 40 nm. The substrates were baked on a hot plate heat 140 °C for 10 min, then transferred into a $N_2$ glovebox. The solution of P3HT (10 mg $mL^{-1}$) in three different solvents DCM, *o*-DCB, and THF (stirred overnight at 50 °C in a $N_2$ glovebox) was spin-coated on the layer of PEDOT:PSS at 3000 rpm for 60s, giving a P3HT buffer layer with the thickness of ca. 30 nm, measured by a Ambios Technology XP-2 profilometer. The film was slowly dried for 2 h at room temperature. Subsequently, the blend solution of P3HT and $PC_{61}BM$ in *ortho*-dichlorobenzene (*o*-DCB) (1:1 w/w, 10 mg $mL^{-1}$ for P3HT:$PC_{61}BM$) was spin-coated on top of the P3HT buffer layer at 1200 rpm for 30 s, then annealed at 150 °C for 10 min on hot plate in a glovebox. The thickness of the photoactive layer was ca. 180 nm. Finally, the negative electrode consisting of LiF (0.8 nm) capped with Al (100 nm) was thermally evaporated onto the active layer under a shadow mask at a base pressure of ca. $10^{-4}$ Pa. The device active area is 4 $mm^2$ for all the PSCs discussed in this work and regulated with a shadow mask. The current–voltage ($I$–$V$) measurements were measured in ambient conditions using a Keithley 2400 source meter unit. The photocurrents were performed under an AM 1.5G illumination at 100 mW·$cm^{-2}$ through an Oriel 96000 150 W solar simulator source. We are using a monocrystalline silicon diode to calibrate the incident light.

**Measurements.** Optical properties were tested by UV–vis spectroscopy (Perkin-Elmer Lambda 750) and a fluorescence spectrometer (Hitachi F-7000). The P3HT: $PC_{61}BM$ blend films (1:1, w/w) and P3HT:$PC_{61}BM$/P3HT films for the UV–visible absorption measurements and fluorescence spectra were prepared on clean quartz glass substrates. The morphologies of P3HT/$PC_{61}BM$ films were investigated by scanning electron microscopy (SEM) using a QuanTA-200F instrument and atomic force microscopy (AFM) using a Digital Instrumental Nanoscope 31 apparatus operated in the tapping mode. X-ray diffraction (XRD) patterns of the samples was carried out on a Bruker D8 Focus X-ray diffractometer operating at 30 kV and 20 mA with a copper target ($\lambda$ =1.54 Å) and at a scanning rate of 1°/min. The procedure used was the same method as that for device fabrication; the P3HT buffer layers were all spin-coated at 5000 rpm for 60s, and the thickness of the P3HT buffer layer was ca. 15 nm, as measured using a Ambios Technology XP-2 profilometer. The thickness of P3HT layers measured constant in all the experiments.

## 3. RESULTS AND DISCUSSION

In order to obtain a thin P3HT film with high degree of crystallinity and prevent this buffer layer dissolution during solution spin-coating process of the active layer, a high-molecular-weight P3HT with a weight-average molecular weight of 48 300 g $mol^{-1}$, head-to-tail regioregularity > 90% was used to prepare such buffer layer by spin-coating from three different solvents, such as DCM, *o*-DCB and THF. Then, the thin P3HT films were allowed slow-drying for two hours at room temperature. Figure 1 displays XRD spectra of the P3HT thin films deposited on ITO from different solvents. All P3HT films show a sharp peak at $2\theta$ = 5.4° (lattice constant 1.635 nm) attribute to the ordered lamellar layer structure (100) of the P3HT plane, proving that the P3HT backbone is parallel to the substrate with an "edge-on" orientation of the thiophene plane.[21] From the spectra we can see that the crystallinity of P3HT films is greatly influenced by the solvents they prepared from. The intensity difference of the reflection peak from the (100) Miller plane implies that the highest degree of crystallinity of P3HT is obtained from THF solution among these three solvents. Generally, the good solvent is favorable for forming the better-ordered molecular packing than the bad one. The solubility of P3HT in these solvents follows DCM < *o*-DCB < THF, which should be responsible for the morphology difference. The observation is good consistent with the results of tapping-mode atomic force microscopy. Figure 2 shows AFM height images (3 $\mu$m × 3 $\mu$m) of P3HT thin films

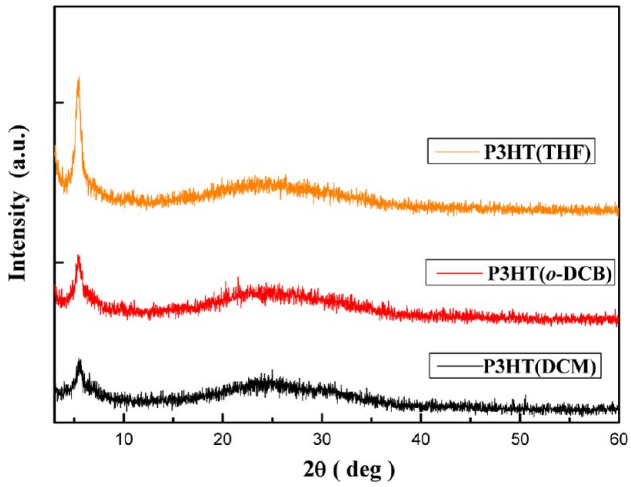


**Figure 1.** X-ray diffraction (XRD) spectra of the P3HT buffer layer prepared from different solvents (DCM, *o*-DCB, and THF).

(prepared from DCM, *o*-DCB, THF). The film casted from DCM reveals a most coarse surface with the root-mean-square (RMS) roughness of 9.96 nm, as shown in Figure 2a. Nevertheless, the films prepared from better solvents, *o*-DCB and THF, the surfaces become smooth and the RMS roughness decreases to 7.01 nm and 2.19 nm, respectively (Figure 2b and c). The decrease of the film roughness is considered to be a signal of enhanced crystallinity in P3HT films.

To clarify whether P3HT layer can undergo the washing of solvent in the process of spin-coating active layer, the hydrophilic property of the PEDOT:PSS/P3HT layer before and after washed by the *o*-DCB was measured by contact angle measurement, as shown in Figure 3. The P3HT layers prepared by DCM, *o*-DCB, and THF solvents show contact angles of 105.5°, 103.5°, and 102.5°, respectively. After washed by *o*-DCB, the contact angles are changed to 34° for DCM, and 60.5° for *o*-DCB. The declined contact angles of P3HT layers prepared by DCM and *o*-DCB are related to the enhanced hydrophilic property after using *o*-DCB washing, implying that the P3HT layers prepared by DCM and *o*-DCB were partly washed away during the process of spin-coating active layer. However, the almost unchanged (99.5°) contact angle of P3HT layers prepared by THF means that the high degree of crystallinity can ensure formation of the P3HT buffer layer not easy to be destroyed and washed away during spin-coating process of the active layer.

A series of polymer solar cells based on this thin P3HT buffer layer with the structure of ITO/PEDOT:PSS/P3HT/P3HT:$PC_{61}BM$/LiF/Al are fabricated to study the impacts of the highly crystalline P3HT layer on device performance. The

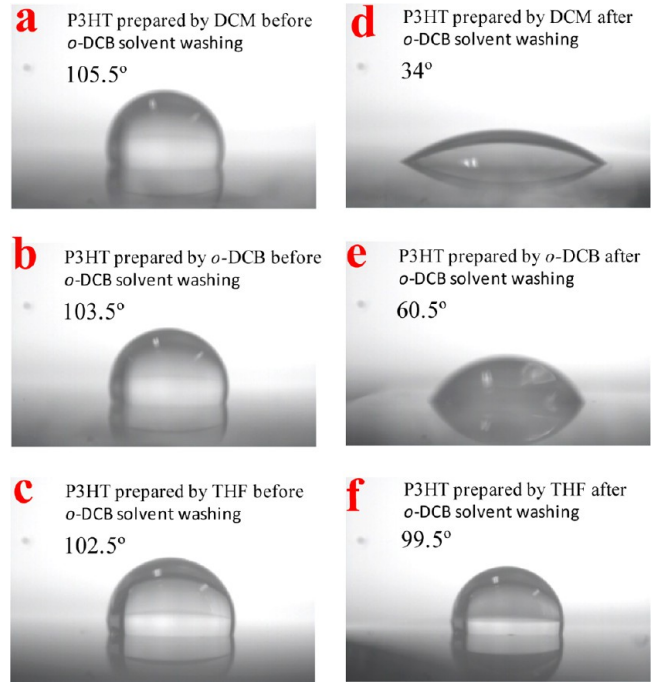


**Figure 3.** Contact angle measurements of the hydrophilic of the PEDOT:POSS/P3HT, which P3HT layer prepared by DCM, *o*-DCB, and THF solvents: (a–c) P3HT layers before using the *o*-DCB solvent washing; (d–f) P3HT layers after using the *o*-DCB solvent washing.

thin P3HT layer with high degree of crystallinity is spin-coated on PEDOT:PSS layer at 3000 rpm for 60s with a concentration of 10 mg $mL^{-1}$, followed by slow drying. Then a layer of P3HT:$PC_{61}BM$ is spin-coated on this P3HT insert layer. As respected, the formation of thin P3HT layer did not be destroyed during the active layer deposition, which can be detected clearly by cross-section SEM image of device presented in Figure 4a. Figure 4b give the current ($J$)–voltage ($V$) characteristics of cells with a P3HT buffer layer prepared from different solvents under AM1.5G illumination at an incident intensity of 100 mW $cm^{-2}$, and that of a control device without such P3HT layer (ITO/PEDOT:PSS/P3HT:$PC_{61}BM$/LiF/Al) is also given for comparison. The photovoltaic data calculated from the $J$–$V$ curves are summarized in Table 1. The control device without P3HT buffer layer exhibits an open-circuit voltage ($V_{oc}$) of 0.651 V, a short-circuit current density ($J_{sc}$) of 8.46 mA·$cm^{-2}$, a fill factor (FF) of 54.1%, and a power conversion efficiency (PCE) of 2.98%. After the inserting a thin P3HT layer between the PEDOT:PSS and P3HT:$PC_{61}BM$ active layer, the cell performance has been remarkably improved, yielding a highest power conversion efficiency of

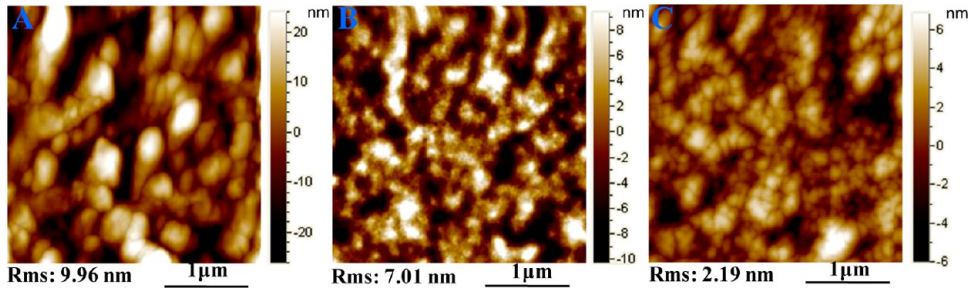


**Figure 2.** Tapping-mode atomic force microscopy height images (3 $\mu$m × 3 $\mu$m) of P3HT layers in different solvents (A, DCM; B, *o*-DCB; C, THF).


dx.doi.org/10.1021/am401863r | ACS Appl. Mater. Interfaces 2013, 5, 5986–5993

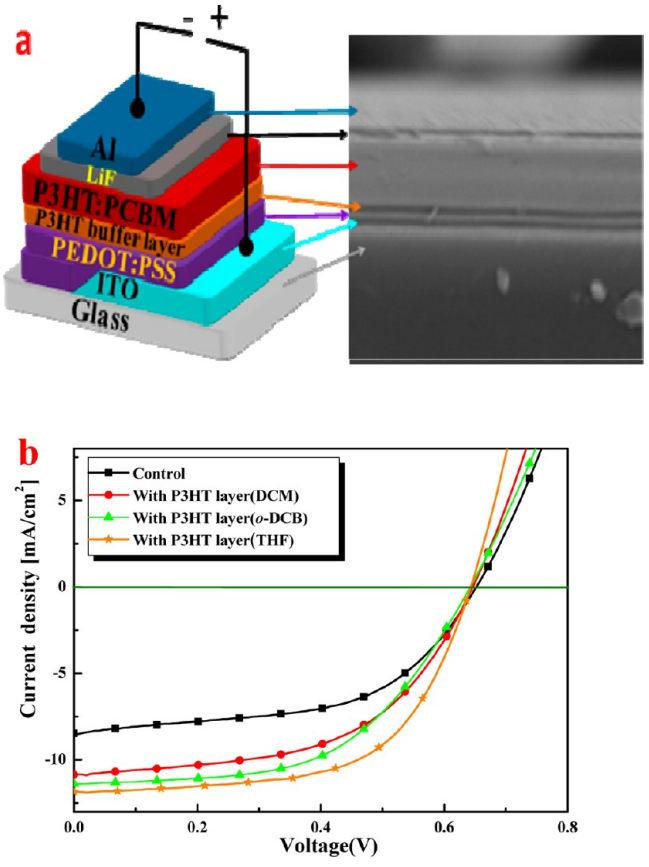


**Figure 4.** (a) Device structure with a cross-sectional SEM image (P3HT buffer layer cast from THF) and (b) the current ($J$)−voltage ($V$) characteristics of cells based on devices without P3HT insert layer (control: ITO/PEDOT:PSS/P3HT:$PC_{61}BM$/LiF/Al) and with a P3HT insert layer cast from different solvents (ITO/PEDOT:PSS/P3HT/P3HT:$PC_{61}BM$/LiF/Al) after thermal annealed at 150 °C.

**Table 1. Device Performance of Solar Cells Incorporating P3HT Buffer Layers from Different Solvents**[ab]

| solvents | $J_{sc}$ (mA·cm$^{-2}$)[c] | $V_{oc}$ (V)[d] | *FF* (%)[e] | PCE (%) |
|---|---|---|---|---|
| DCM | 10.86 | 0.645 | 55.7 | 3.90 |
| *o*-DCB | 11.40 | 0.642 | 56.6 | 4.14 |
| THF | 11.90 | 0.643 | 61.6 | 4.71 |
| without P3HT[f] | 8.46 | 0.651 | 54.1 | 2.98 |

[a]Under A.M. 1.5, 100 mW/cm$^2$ irradiation. [b]All values represent averages from six 4 mm$^2$ devices on a single chip. [c]$J_{sc}$ is the short circuit current. [d]$V_{oc}$ is the open-circuit voltage. [e]The fill factor (FF) is a graphic measure of the squareness of the $J$−$V$ curve. [f]The results for comparison are the device without P3HT buffer layer.

4.71% for the device with a P3HT layer prepared from THF solution. Inset of P3HT buffer layer slightly increases FF and has a minor effect on the $V_{oc}$, but dramatically improves the value of $J_{sc}$, which is in good agreement with the observation reported by literatures.[19,20]

Several effects that influenced the $J_{sc}$ values as a function of P3HT layer were identified.[19,20] One contribution arose from the P3HT layer creating new contacts with those $PC_{61}BM$ molecules distributed near the bottom of the P3HT:$PC_{61}BM$ film, therefore, increasing the rate of generation of free carriers and the photocurrent density. Second, this layer substantially enhanced the electron blocking capability of PEDOT:PSS, leading to the reduction of charge combination. In addition, the enhance value of $J_{sc}$ is in correlation with the P3HT buffer layer increase the extra solar flux absorption. It is worth noting that incorporation of the P3HT layer increased $J_{sc}$ value by about 28% to 10.86 mA·cm$^{-2}$ (from DCM), 35% to 11.40 mA·cm$^{-2}$ (from *o*-DCB), 41% to 11.90 mA·cm$^{-2}$ (from THF). Despite of the solvent for P3HT underlying layer preparation, all devices were fabricated under the same conditions. The different enhancement of current density in the devices with P3HT thin layer casted from different solvent should be definitely related to the crystallinity of the P3HT underlying layer, which is the only aspect that the solvent influenced. Therefore, we can conclude that, in addition to the reasons behind the $J_{sc}$ enhancement mentioned above, the morphology change of active layer induced by such tiny thin P3HT layer is also a very important factor to influence current density. When spin-coating P3HT:$PC_{61}BM$ composite on the tiny P3HT layer, the highly ordered structure of P3HT acted as a function of crystal seeds to induce the polymer chain in upper active layer packing with a better formation, which offered a more favorable pathway for charge separation and transportation. Figure 5

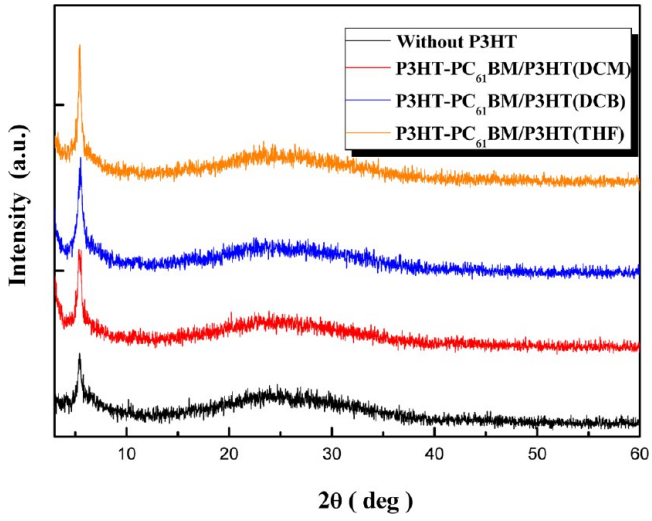


**Figure 5.** XRD spectra of the active layer before and after insert a P3HT layer prepared from different solvent.

interprets the improved crystalline of the P3HT in active layer by comparing the relative intensities at a specific position ($2\theta$ = 5.4°) of the X-ray diffraction spectra. Compared to P3HT:$PC_{61}BM$ film, an obvious enhancement in lamellar packing can be detected in P3HT:$PC_{61}BM$ films with P3HT layer, and it also shows a strong dependence on the solvent used for P3HT underlying layer preparation. This result is the outstanding consequence of the enhanced crystalline of P3HT in active layer via well-organization induced by P3HT insert layer. Scheme 1 summarizes our comprehension of the morphological evolution for P3HT:$PC_{61}BM$ binary by insetting such P3HT underlying layer.

UV−vis absorption spectrum was applied to explore the effect of P3HT layer on the morphology and light absorption of P3HT:$PC_{61}BM$ composite, as shown in Figure 6a. All the UV−vis absorption spectra of P3HT/P3HT:$PC_{61}BM$ with P3HT base layer included the higher optical density than that of the P3HT:$PC_{61}BM$ without P3HT base layer in the whole wavelength range. It was suggested that the incorporation of P3HT buffer layer significantly increased the light absorption, which is maybe attribute to the redistribution of optical electric-


dx.doi.org/10.1021/am401863r | ACS Appl. Mater. Interfaces 2013, 5, 5986−5993

**Scheme 1. Morphological Evolution for P3HT:$PC_{61}BM$ Binary by Insetting P3HT Buffer Layer**

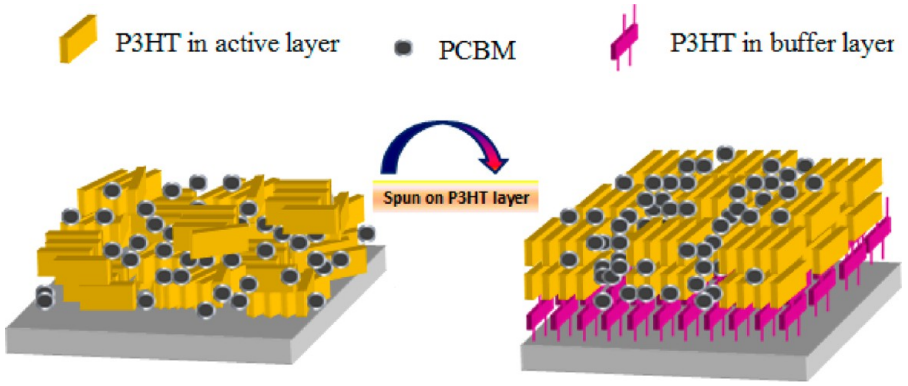


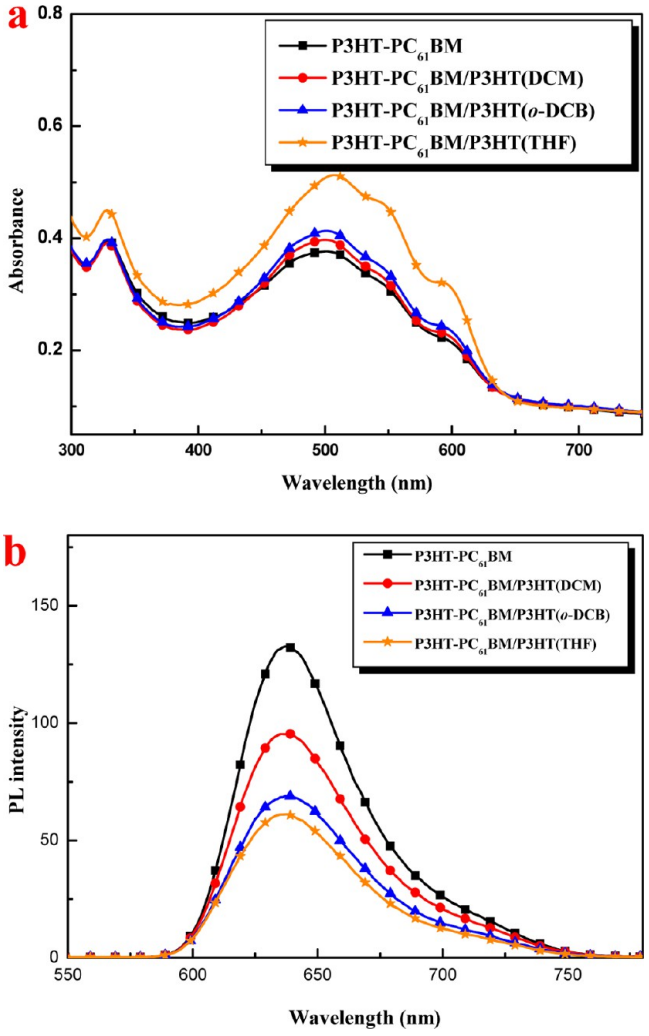


**Figure 6.** (a) UV−visible absorption spectra and (b) photoluminescence spectra of P3HT-$PC_{61}BM$ and P3HT-$PC_{61}BM$/P3HT (from different solvents) films on a quartz plate.

field. Evidently, among these films, the one casted from THF solution showed the strongest absorption and most pronounced vibronic shoulders at the wavelengths of 550 and 600 nm. This peak is common for P3HT thin films and generally is ascribed to the interchain vibrational absorption induced by a high degree of ordering and strong interchain interaction.[22,23] In addition, the different enhancement of absorption with P3HT thin layer casted from different solvent should be definitely related to the crystallinity of the P3HT underlying layer, which is the only aspect that the solvent influenced. Thus, we refer that the enhanced light absorption not only came from the redistribution of optical electric-field of P3HT layer, but also could be attributed to the improved crystallinity of P3HT in the active layer. The increased light absorption improved the efficiency and $J_{SC}$. The well self-assembled active layer morphology induced by insetting such a thin layer has also been supported by the photoluminescence spectra of films measured at an excitation wavelength of 460 nm, presented in Figure 6b. The emission intensity of P3HT:$PC_{61}BM$ clearly exceeded that of P3HT (from different solvents)/P3HT:$PC_{61}BM$, although the latter has higher absorbance at the excitation wavelength, especially for the THF-cast P3HT/P3HT:$PC_{61}BM$ film. This finding elucidates that the P3HT layer not only created new interfacial area between the donor and the acceptor to increase charge generation, but also enhanced the more efficient charge transportation by forming a more ordered pathway to the electrodes.

For greater clarity, SEM was performed on both P3HT/$PC_{61}BM$ and P3HT:$PC_{61}BM$/P3HT films spin-coated on the ITO/PEDOT:PSS substrate. A P3HT thin layer brought a significant morphological change on P3HT:$PC_{61}BM$ blend film, shown in Figure 7. Quite different from P3HT:$PC_{61}BM$ film without P3HT underlying layer, a distinct lamellar structure was formed in P3HT:$PC_{61}BM$ blend film after inserting a P3HT buffer layer, especially in the case of P3HT layer prepared from THF. The lamellar structure was observed at the length scale of few hundred nanometers, which is a reflection of a well-packed in P3HT:$PC_{61}BM$ composite induced by the underlying buffer layer, that is, the internal orderly arrangement led to a distinct lamellar structure on the external morphology. Nevertheless, for P3HT:$PC_{61}BM$ with DCM-induced P3HT layer, the lamellar structure was not developed so well with respect to the others, probably because the surface of P3HT thin film has been partly dissolved during the active layer coating process, due to its relatively low crystalline.

Corresponding changes in the surface topography of the P3HT:$PC_{61}BM$ blend films with and without a P3HT underlying layer were also seen by atomic force microscopy. Insert of P3HT buffer layer led to a pronounced morphology change on P3HT/$PC_{61}BM$ films compared with the film without a P3HT buffer layer (Figure 8). The impact of solvent on morphology can be illustrated by the surface root-mean-square roughness of P3HT/$PC_{61}BM$. The decrease in roughness (2.34 nm for film with insert layer cast from DCM, 0.95 nm for film with insert layer cast from *o*-DCB, and 0.75 nm for


dx.doi.org/10.1021/am401863r | ACS Appl. Mater. Interfaces 2013, 5, 5986−5993

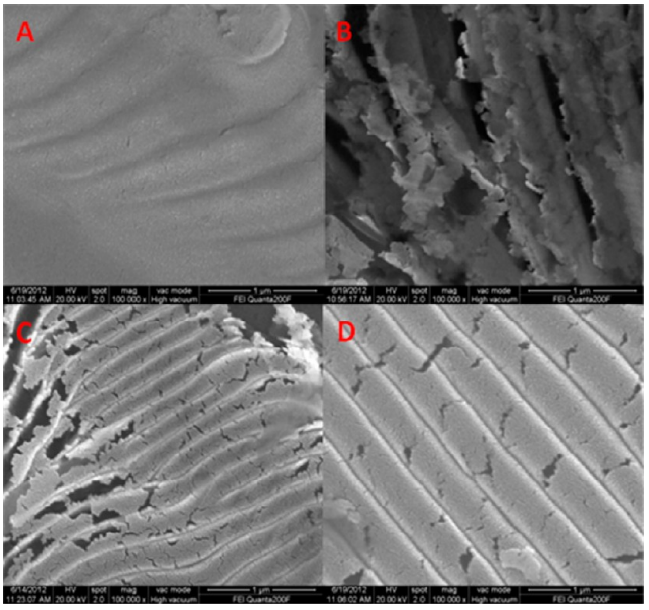


**Figure 7.** SEM images of P3HT/$PC_{61}BM$ films (A) without P3HT buffer layer, (B) with P3HT buffer layer prepared from DCM, (C) with P3HT buffer layer prepared from *o*-DCB, and (D) with P3HT buffer layer prepared from THF.

film with insert layer cast from THF) indicated that the crystallinity of P3HT buffer layer greatly influenced the physical interactions between the polymer chains and/or between the polymer and fullerene phases in active layer. The high crystallinity of the P3HT insert layer caused the P3HT:$PC_{61}BM$ well-packing, consequently favoring the active layer to form a well-ordered interpenetrating network for charge transfer and transportation.

Among these three solvent, THF is most favorable for P3HT to obtain the highest degree of crystallinity, thus yielding the highest $J_{sc}$ and PCE. Further improvement in PCE occurred after optimizing the thickness of the P3HT insert layer cast from THF. The effect of the thickness on the photovoltaic performance of the PSCs was studied by varying the spin-coating revolutions from 800 to 6000 rpm. Figure 9a plots the current density−voltage ($J$−$V$) curves of the PSCs based on P3HT:$PC_{61}BM$ (1:1, w/w) with P3HT layer prepared at different spin-coating revolutions, under the illumination of AM 1.5G, 100 mW $cm^{-2}$. Device current density/voltage ($J$−$V$) characteristics and the parameters are listed in Table 2. For the seven PSC devices with P3HT buffer layer, $V_{oc}$ kept almost constant in the range of 0.630−0.651 V. At the same time, the FF of the PSCs slightly improved to 62.2% with the revolution increases. Interestingly, the $J_{sc}$ of the PSC devices changed significantly with the spin-coating revolution. As the revolution varied from 800 to 5000 rpm, the photocurrent increased from 10.1 to 12.9 mA·$cm^{-2}$, yielding the highest PCE of 5.14% for device with 5000 rpm. One reasonable explanation for this variation is a low revolution produced a thick P3HT film, which made the series resistance ($R_s$) value increase from 30.24 to 56.52 Ω·$cm^2$. The increasing resistance causes a decrease in FF, which is partly determined by $R_s$.[20,24,25] The improved $J_{sc}$ and efficiency has also been determined by the incident phototo-electron conversion efficiency spectrum (IPCE) of solar cell with 5000 rpm (Figure 9b). The profile of IPCE is similar to the UV−vis spectrum, and the P3HT/$PC_{61}BM$ device processed with P3HT layer displayed significantly enhanced IPCEs relative to that without P3HT layer. Further increasing the revolution to 6000 rpm made the $J_{sc}$ quickly decrease to

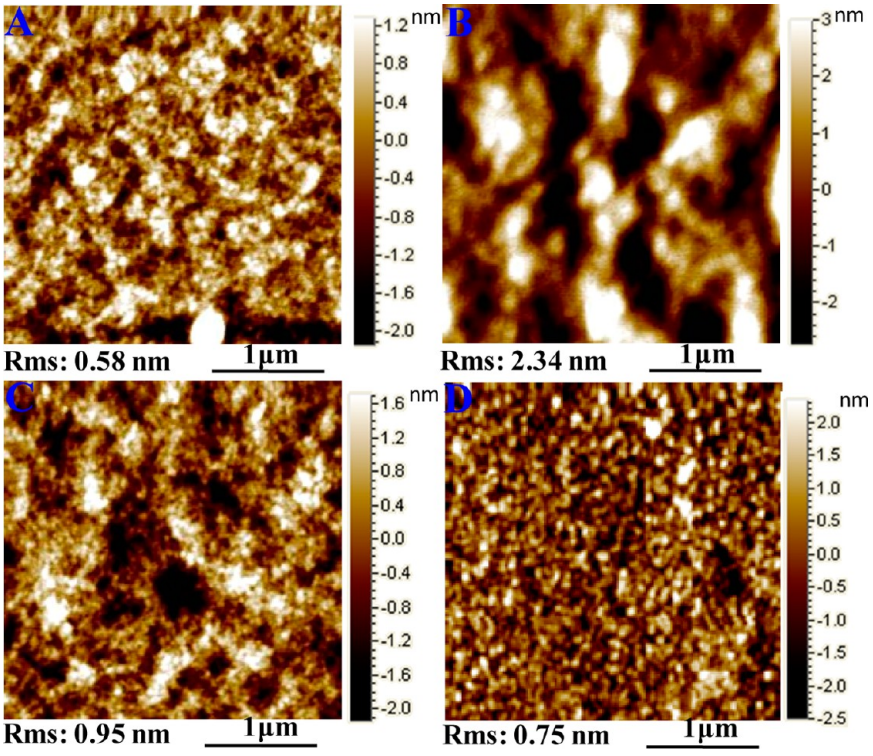


**Figure 8.** Tapping-mode AFM height images (3 μm × 3 μm) of active layers (A) without P3HT buffer layer or (B−D) with the P3HT buffer layer prepared from different solvents (B, DCM; C, *o*-DCB; D, THF).

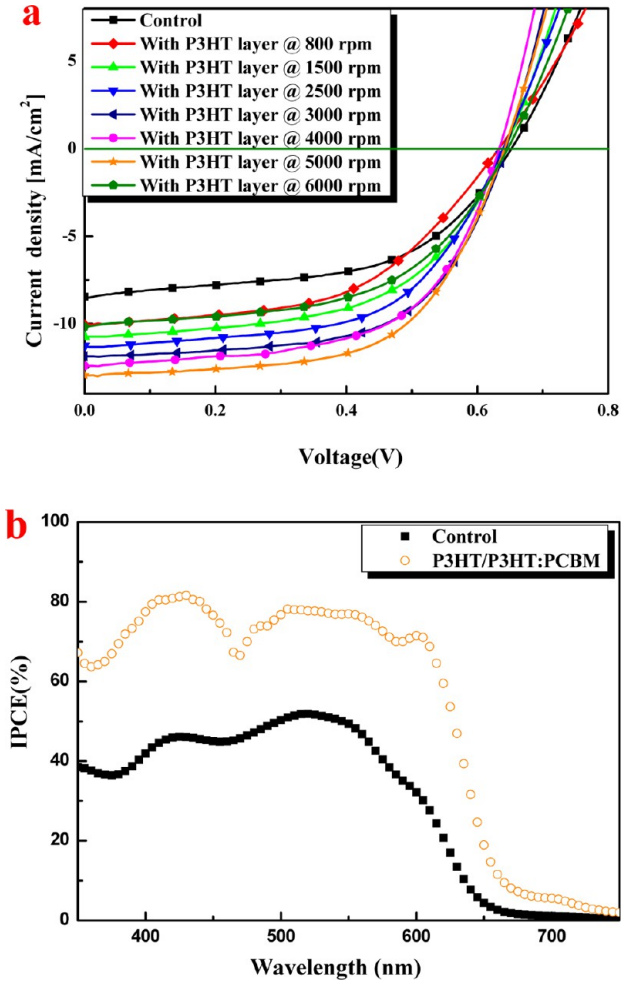


**Figure 9.** (a) $J-V$ characteristics of photovoltaic cells based on devices without a P3HT layer (Control: ITO/PEDOT:PSS/P3HT:$PC_{61}BM$/LiF/Al) and with a P3HT layer prepared from THF (ITO/PEDOT:PSS/P3HT/P3HT:$PC_{61}BM$/LiF/Al) at different thickness. (b) Incident photon-to-current efficiency (IPCE) of photovoltaic cells based on cells of control and buffer layer with 5000 rpm.

**Table 2. Device Performance of Solar Cells Incorporating P3HT Buffer Layers Cast from THF with Various Thicknesses, Controlled by Varying the Revolutions Per Minute during Spin Coating[ab]**

| thickness (rpm) | $J_{sc}$ (mA·cm$^{-2}$)[c] | $V_{oc}$ (V)[d] | FF (%)[e] | PCE (%) | $R_s$ (Ω·cm$^2$) |
|---|---|---|---|---|---|
| control[f] | 8.46 | 0.651 | 54.1 | 2.98 | 42.36 |
| 800 | 10.1 | 0.630 | 50.8 | 3.18 | 56.52 |
| 1500 | 10.7 | 0.641 | 52.9 | 3.63 | 47.67 |
| 2500 | 11.3 | 0.639 | 57.8 | 4.17 | 37.65 |
| 3000 | 11.9 | 0.643 | 61.6 | 4.71 | 31.17 |
| 4000 | 12.4 | 0.634 | 61.1 | 4.80 | 31.45 |
| 5000 | 12.9 | 0.641 | 62.2 | 5.14 | 30.24 |
| 6000 | 10.2 | 0.645 | 53.9 | 3.55 | 43.12 |

[a]Under A.M. 1.5, 100 mW/cm$^2$ irradiation. [b]All values represent averages from six 0.04 cm2 devices on a single chip. [c]$J_{sc}$ is the short circuit current. [d]$V_{oc}$ is the open-circuit voltage. [e]The fill factor (FF) is a graphic measure of the squareness of the $J-V$ curve. [f]The control one for comparison is the device without P3HT buffer layer.

10.2% with a efficiency of 3.55%, probably due to the too high revolution resulting in the surface of the PEDOT:PSS layer not fully covered by the P3HT, eventually leading to a sharp decreased performance.

The relative values of IPCE and $J_{sc}$ could be calculated by expression as reference.[26] The devices contain an inserted hole-transport layer between electrode and active layer in this application, which are different from the structures as reference. The generation efficiency of excitions is not probably applicable to the expression. IPCE of approximate 80% was obtained while $J_{sc}$ was 12.9 mA cm$^{-2}$ in this device.

## 4. CONCLUSIONS

In summary, we demonstrate an useful and convenient method for controlling the morphology and crystallinity of P3HT:$PC_{61}BM$ blend films by simply precasting a tiny, thin P3HT layer with high crystallinity between PEDOT:PSS and photoactive layers. The influence of crystallinity of P3HT buffer layer on morphology of the P3HT:$PC_{61}BM$ composites and photovoltaic performances are focused. The crystallinity of P3HT buffer layer greatly impacted on the physical interactions between the polymer chains and/or between the polymer and fullerene phases in active layer. The high crystallinity of P3HT insert layer consequently favored the active layer to form well-ordered interpenetrating network for charge transfer and transportation. Among those solvents for P3HT insert layer preparation, THF is found to be most favorable for the thin layer to obtain the highest degree of crystallinity, thus yielding the highest $J_{sc}$ of 12.9 mA·cm$^{-2}$, yielding the highest PCE of 5.14%.

## AUTHOR INFORMATION

### Corresponding Author

*Tel.: +86 791 83969562. Fax: +86 791 83969561. E-mail: ywchen@ncu.edu.cn.

### Notes

The authors declare no competing financial interest.

## ACKNOWLEDGMENTS

This work was supported by the National Natural Science Foundation of China (51073076, 51273088, 51003045, and 51263016).

## REFERENCES

(1) Arias, A. C.; MacKenzie, J. D.; McCulloch, I.; Rivnay, J.; Salleo, A. *Chem. Rev.* **2010**, *110*, 3−24.
(2) Kim, J. Y.; Kim, S. H.; Lee, H. H.; Lee, K.; Ma, W.; Gong, X.; Heeger, A. J. *Adv. Mater.* **2006**, *18*, 572−576.
(3) Hoppe, H.; Sariciftci, N. S. *J. Mater. Chem.* **2006**, *16*, 45−61.
(4) Moulé, A. J.; Meerholz, K. *Adv. Mater.* **2008**, *20*, 240−245.
(5) Moulé, A. J.; Meerholz, K. *Adv. Funct. Mater.* **2009**, *19*, 3028−3036.
(6) Yang, X.; Loos, J.; Veenstra, S. C.; Verhees, W. J. H.; Wienk, M. M.; Kroon, J. M.; Michels, M. A. J.; Janssen, R. A. J. *Nano Lett.* **2005**, *5*, 579−583.
(7) Mihailetchi, V. D.; Xie, H. X.; de Boer, B.; Koster, L. J. A.; Blom, P. W. M. *Adv. Funct. Mater.* **2006**, *16*, 699−708.
(8) Caironi, M.; Agostinelli, T.; Natali, D.; Sampietro, M.; Cugola, R.; Catellani, M.; Luzzati, S. *J. Appl. Phys.* **2007**, *102*, 024503.
(9) Campoy-Quiles, M.; Ferenczi, T.; Agostinelli, T.; Etchegoin, P. G.; Kim, Y.; Anthopoulos, T. D.; Stavrinou, P. N.; Bradley, D. D. C.; Nelson, J. *Nat. Mater.* **2008**, *7*, 158−164.
(10) Chen, L.-M.; Hong, Z.; Li, G.; Yang, Y. *Adv. Mater.* **2009**, *21*, 1434−1449.
(11) Ma, W.; Yang, C.; Gong, X.; Lee, K.; Heeger, A. J. *Adv. Funct. Mater.* **2005**, *15*, 1617−1622.

(12) Li, G.; Yao, Y.; Yang, H.; Shrotriya, V.; Yang, G.; Yang, Y. *Adv. Funct. Mater.* **2007**, *17*, 1636−1644.
(13) Yao, Y.; Hou, J.; Xu, Z.; Li, G.; Yang, Y. *Adv. Funct. Mater.* **2008**, *18*, 1783−1789.
(14) Pivrikas, A.; Stadler, P.; Neugebauer, H.; Sariciftci, N. S. *Org. Electron.* **2008**, *9*, 775−782.
(15) Xu, Z.; Chen, L.-M.; Yang, G.; Huang, C.-H.; Hou, J.; Wu, Y.; Li, G.; Hsu, C.-S.; Yang, Y. *Adv. Funct. Mater.* **2009**, *19*, 1227−1234.
(16) Liao, H.-H.; Chen, L.-M.; Xu, Z.; Li, G.; Yang, Y. *Appl. Phys. Lett.* **2008**, *92*, 173303.
(17) Wei, Q.; Nishizawa, T.; Tajima, K.; Hashimoto, K. *Adv. Mater.* **2008**, *20*, 2211−2216.
(18) Kumar, A.; Li, G.; Hong, Z.; Yang, Y. *Nanotechnology* **2009**, *20*, 165202.
(19) Liang, C.-W.; Su, W.-F.; Wang, L. *Appl. Phys. Lett.* **2009**, *95*, 133303.
(20) Wei, H.-Y.; Huang, J.-H.; Ho, K.-C.; Chu, C.-W. *ACS Appl. Mater. Interfaces* **2010**, *2*, 1281−1285.
(21) Erb, T.; Zhokhavets, U.; Gobsch, G.; Raleva, S.; Stühn, B.; Schilinsky, P.; Waldauf, C.; Brabec, C. J. *Adv. Funct. Mater.* **2005**, *15*, 1193−1196.
(22) Kim, Y.; Cook, S.; Tuladhar, S. M.; Choulis, S. A.; Nelson, J.; Durrant, J. R.; Bradley, D. D. C.; Giles, M.; McCulloch, I.; Ha, C.-S.; Ree, M. *Nat. Mater.* **2006**, *5*, 197−203.
(23) Brown, P.; Thomas, D.; Köhler, A.; Wilson, J.; Kim, J.-S.; Ramsdale, C.; Sirringhaus, H.; Friend, R. *Phys. Rev. B* **2003**, *67*, 064203.
(24) Nelson, J. Imperial College Press: London, 2002.
(25) Kim, H.; So, W. W.; Moon, S. J. *J. Korean Phys. Soc.* **2006**, *48*, 441−445.
(26) Dennler, G.; Scharber, M. C.; Brabec, C. J. *Adv. Mater.* **2009**, *21*, 1323−1338.